Supplementary information

Binary solvent-mediated modulation of two-dimensional nanoconfined catalytic behaviors

Haoran Shi,[a,b] Xiaotao Yang,[c] Xinxin Cui,[a,b] Hongyan Xiao,[a] Shuai Pang,[c] Xiang Li,[a,b] Yue Long,[a*] Xiqi Zhang,[a,c*] Kai Song[a,b*] and Lei Jiang[a,b,c]

[a] *Laboratory of Bio-inspired Smart Interface Science, Technical Institute of Physics and Chemistry, Chinese Academy of Sciences, Beijing 100190, P. R. China.*
[b] *School of Future Technology, University of Chinese Academy of Sciences, Beijing 100049, P. R. China.*
[c] *Suzhou Institute for Advanced Research, University of Science and Technology of China, Jiangsu 215123, P. R. China.*

CONTENTS

Molecular dynamics simulations.

Based on the experimental conditions, a simplified model of GO with an oxidation degree of 47% was built, in which hydroxyl and epoxy groups were randomly distributed on both sides of the graphene in a ration of 3:2.[1] The size of the GO membrane model was set to 15.25 nm×4.26 nm. In two parallel GO membranes with different interlayer distance, different proportions of solvents were filled to simulate the actual situation using Packmol package.[2] The detailed system composition was shown in Table S1.

All-atom OPLS-AA force field was used in these simulations.[3] The force field parameters of GO referred to our previous work and references therein.[4,5] The detailed simulation steps were as follows: (1) the initial model was energy-minimized in order to remove the system strain; (2) 200 ps constrained dynamics simulations were tested and carried out in which the carbon atoms on GO were restrained and the initial velocities were generated based on a Maxwellian distribution at 297.15 K at NVT canonical ensemble; (3) 10 ns constrained dynamics simulations were performed, where sampling analyses of last 3 ns NVT MD simulations were used. All the bonds with H-atoms were constrained by the LINCS algorithm and a time step of 1.0 fs was used in all the simulations. The temperature was controlled using the velocity-rescaling thermostat with a relaxation time of 0.1 ps. Particle mesh Ewald (PME) summation method was used to calculate the electrostatic potential under periodic boundary condition in all three spatial dimensions. The cut-off method was employed to calculate the Van der Waals potential as 1.4 nm. We examined the variations of potential energy, kinetic energy and temperature over time to ensure the balance of the system. All the MD simulations were performed with the GROMACS 2018.1 package.[6-12]

System	GO			
	EtOH-DMF binary solvent			
EtOH content	100%	70%	50%	30%
interlayer distance (nm)	1.09	1.24	1.48	1.59
Molecule number	503	422/136	382/288	252/442
HB number of GO	610.5	600.2	614.2	616.9
HB number between GO and binary solvent	284.6	277.9	237.9	190.1
Average HB number between GO and binary solvent	1.1	1.0	0.7	0.5
Average HB number of EtOH	1.3	1.0	1.0	0.7
Average HB number of binary solvents	1.3	1.0	0.8	0.5

Table S1 System composition and hydrogen bond number. The criterion for forming H-bonds is that the donor-acceptor distance is less than 0.35 nm and the hydrogen-donor-acceptor angle is less than 30°.

Fig. S1. Photograph of th

Fig. S2. XPS spectrum for eak can be fitted by four peaks at 284.8, 286.5, 287.0, and 2 C(sp2), C–O, C=O, and C(O)O, respectively.

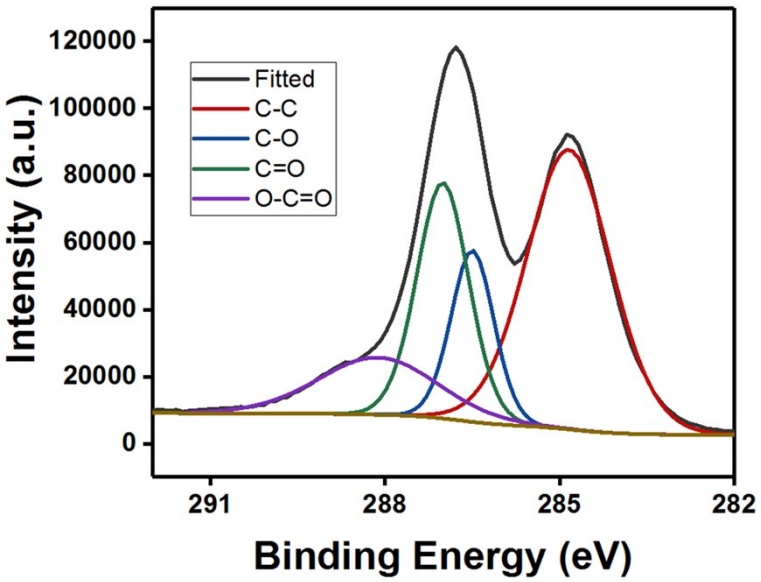

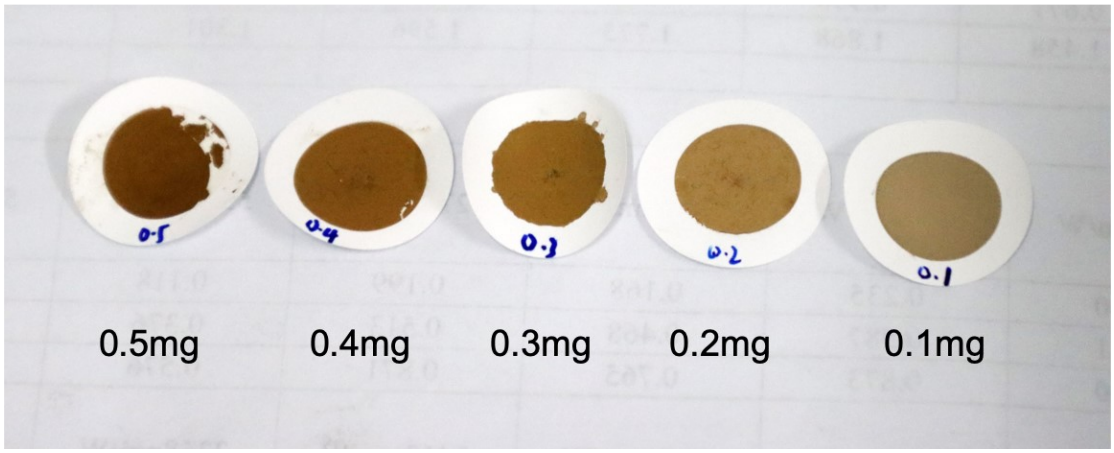

Fig. S3. **Photograph of a list of GO membranes fabricated by GO powder of 5 different weight.** The thickness of GO membranes of each amounts: 0.5 mg: 1.4 µm; 0.4 mg: 1.2 µm; 0.3 mg: 1.0 µm; 0.2 mg: 0.9 µm; 0.1 mg: 0.8 µm.

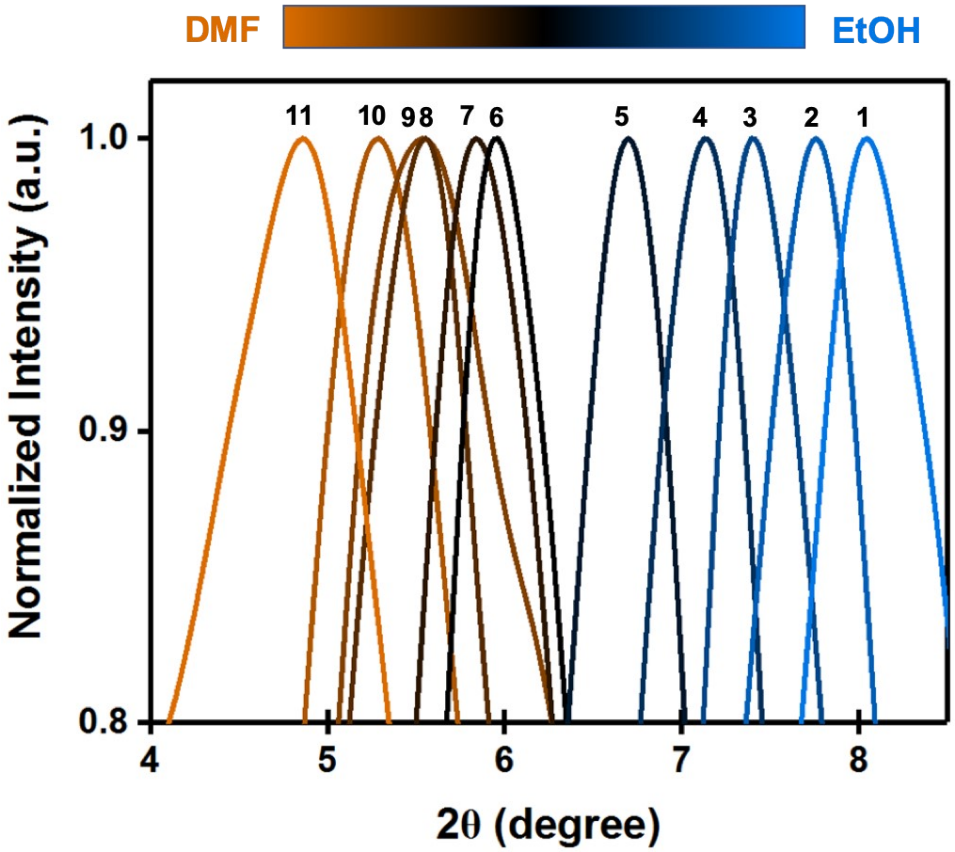

Fig. S4. **XRD patterns of GO films measured in the EtOH-DMF binary solvent**. The blue and orange curves represent the XRD patterns obtained from GO films in EtOH and DMF, respectively. While the transition from blue to orange indicates a decrease in the ED ratio. Peaks: 1-EtOH-10.9Å; 2-EtOH-DMF (9:1)-11.6 Å; 3-EtOH-DMF (8:2)-12.0 Å; 4-EtOH-DMF (7:3)-12.4 Å; 5- EtOH-DMF (6:4)-13.2 Å; 6-EtOH-DMF (5:5)-14.8 Å; 7-EtOH-DMF (4:6)-15.1 Å; 8-EtOH-DMF (3:7)-15.9 Å; 9- EtOH-DMF (2:8)-16.0 Å; 10- EtOH-DMF (1:9)-16.7 Å; 11-DMF-18.2 Å.

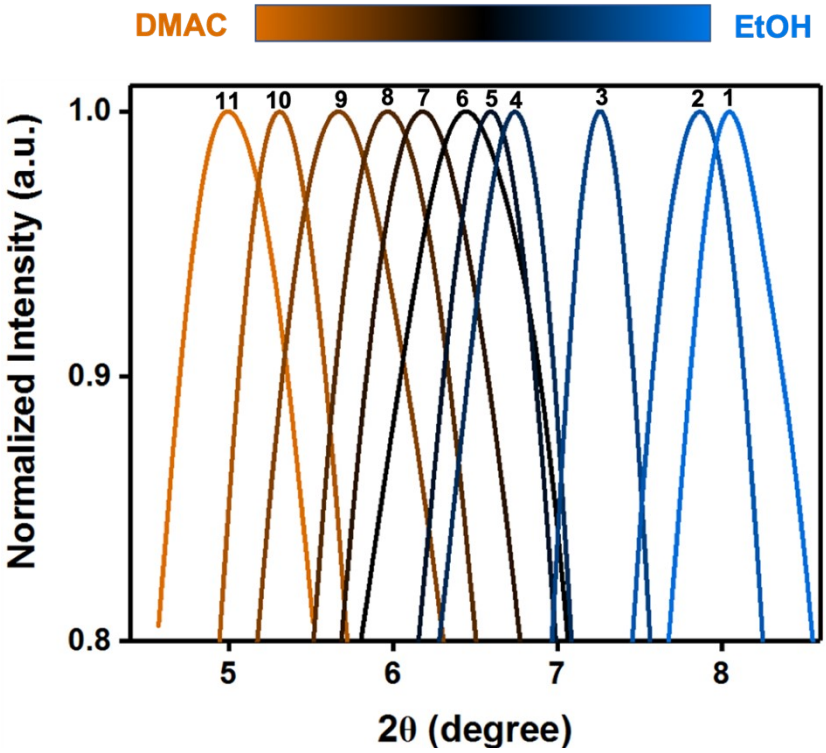

Fig. S5. **XRD patterns of GO films measured in the EtOH-DMAC binary solvent.** The blue and orange curves represent the XRD patterns obtained from GO films in EtOH and DMAC, respectively. While the transition from blue to orange indicates a decrease in the ED ratio. Peaks: 1-EtOH-10.9Å; 2-EtOH-DMAC (9:1)-11.2 Å; 3-EtOH-DMAC (8:2)-12.2 Å; 4-EtOH-DMAC (7:3)-13.1 Å; 5-EtOH-DMAC (6:4)-13.4 Å; 6-EtOH-DMAC (5:5)-13.7 Å; 7-EtOH-DMAC (4:6)-14.3 Å; 8-EtOH-DMAC (3:7)-14.8 Å; 9-EtOH-DMAC (2:8)-15.6 Å; 10-EtOH-DMAC (1:9)-16.6 Å; 11-DMAC-17.7 Å

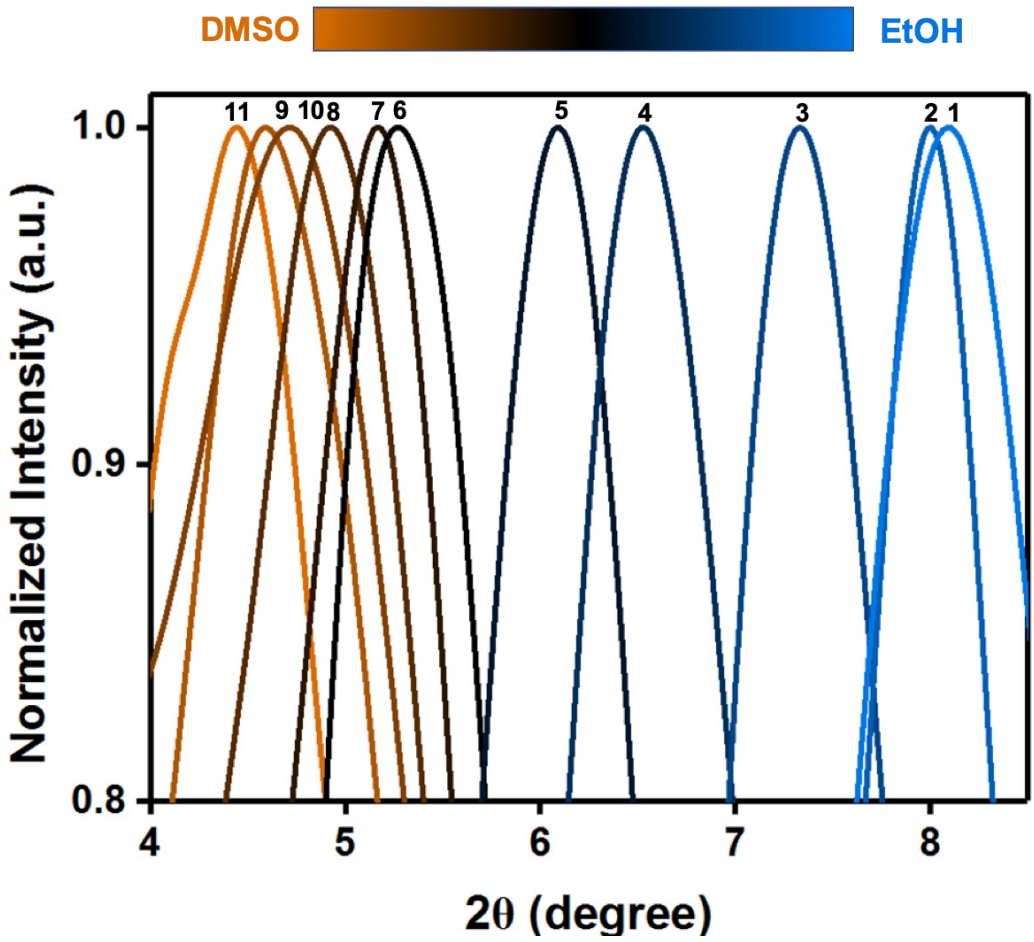

Fig. S6. **XRD patterns of the GO membranes in EtOH-DMSO binary solvent.** The blue and orange curves represent the XRD patterns obtained from GO films in EtOH and DMSO, respectively. while the transition from blue to orange indicates a decrease in the ES ratio. Peaks: 1-EtOH-10.9 Å; 2-EtOH-DMSO (9:1)-11.0 Å; 3-EtOH-DMSO (8:2)-12.0 Å; 4-EtOH-DMSO (7:3)-13.5 Å; 5-EtOH-DMSO (6:4)-14.5 Å; 6-EtOH-DMSO (5:5)-16.7 Å; 7-EtOH-DMSO (4:6)-17.1 Å; 8-EtOH-DMSO (3:7)-18.0 Å; 9-EtOH-DMSO (2:8)-18.7 Å; 10-EtOH-DMSO (1:9)-18.2 Å; 11-DMSO-19.9 Å.

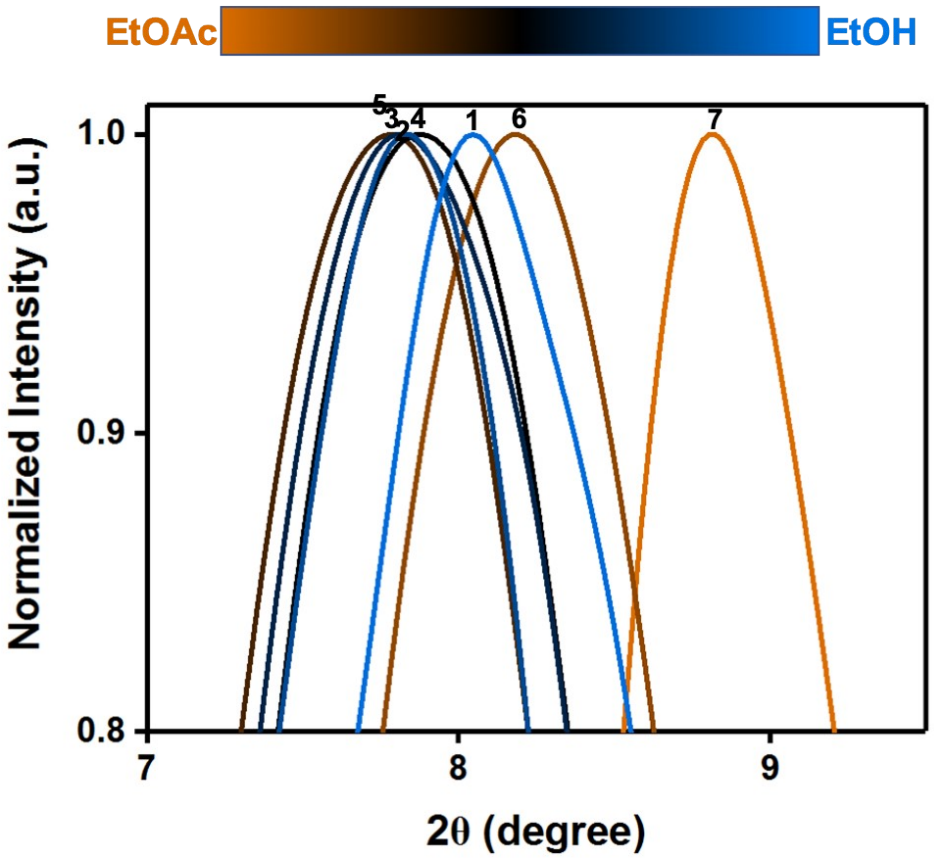

Fig. S7. XRD patterns of the GO membranes in EtOH-EtOAc binary solvent. The blue and orange curves represent the XRD patterns obtained from GO films in EtOH and EtOAc, respectively. While the transition from blue to orange indicates a decrease in the EA ratio. Peaks: 1-EtOH-10.9 Å; 2-EtOH-EtOAc (9:1)-11.3 Å; 3-EtOH-EtOAc (7:3)-11.3 Å; 4-EtOH-EtOAc (5:5)-11.2 Å; 5- EtOH-EtOAc (3:7)-11.4 Å; 6-EtOH-EtOAc (1:9)-10.8 Å; 7- EtOAc -10.0 Å.

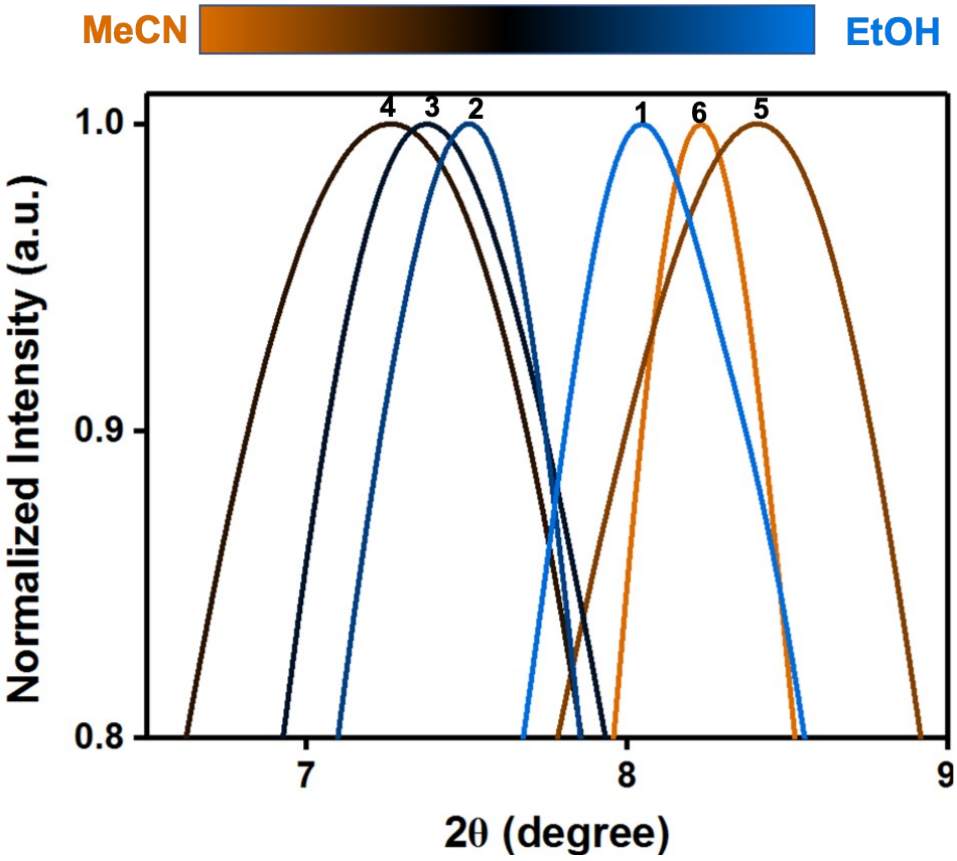

Fig. S8. **XRD patterns of the GO membranes in EtOH-MeCN binary solvent.** The blue and orange curves represent the XRD patterns obtained from GO films in EtOH and MeCN, respectively. while the transition from blue to orange indicates a decrease in the EM ratio. Peaks: 1-EtOH-10.9 Å; 2-EtOH-MeCN (9:1)-11.8 Å; 3-EtOH-MeCN (7:3)-12.0 Å; 4-EtOH-MeCN (5:5)-12.1 Å; 5-EtOH-MeCN (3:7)-10.5 Å; 6-MeCN-10.7 Å.

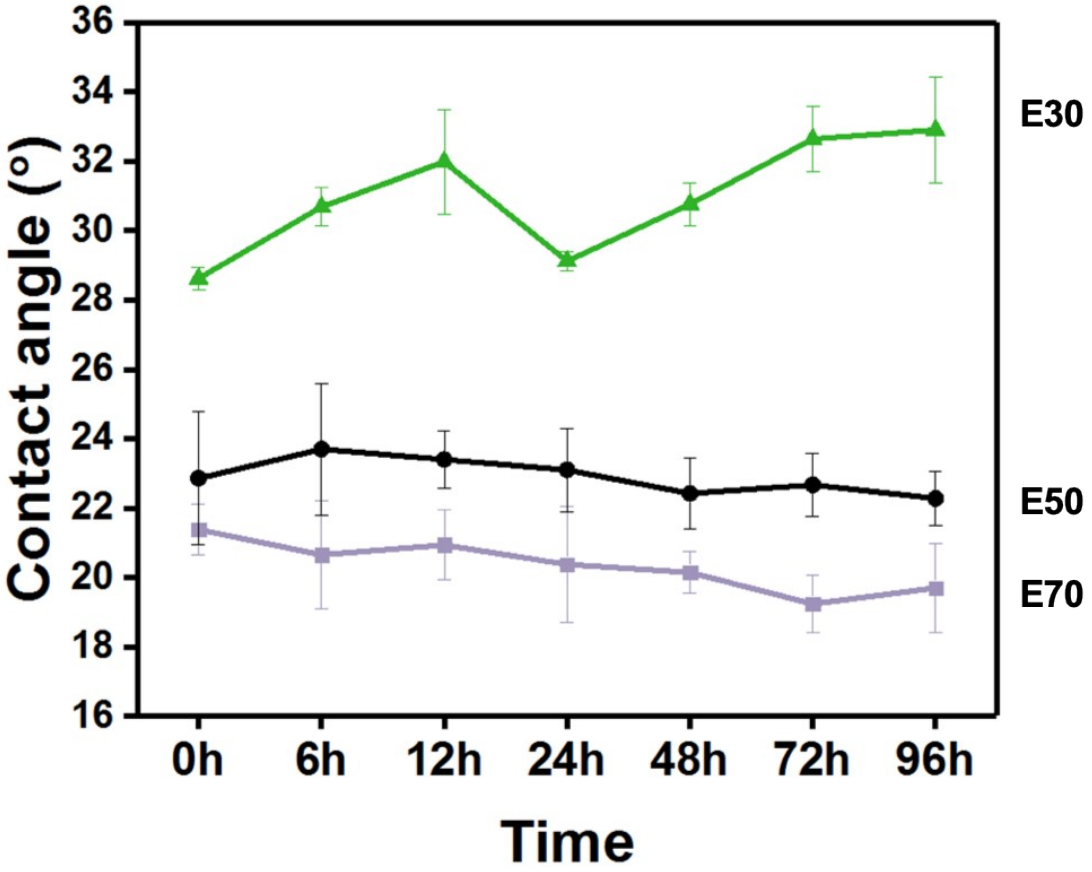

Fig. S9. **CA of EtOH-DMF binary solvent stabilized for 6h, 12, 24h. 48h, 72h and 96h, respectively.** 30%, 50% and 70% ethanol content were measured as the example.

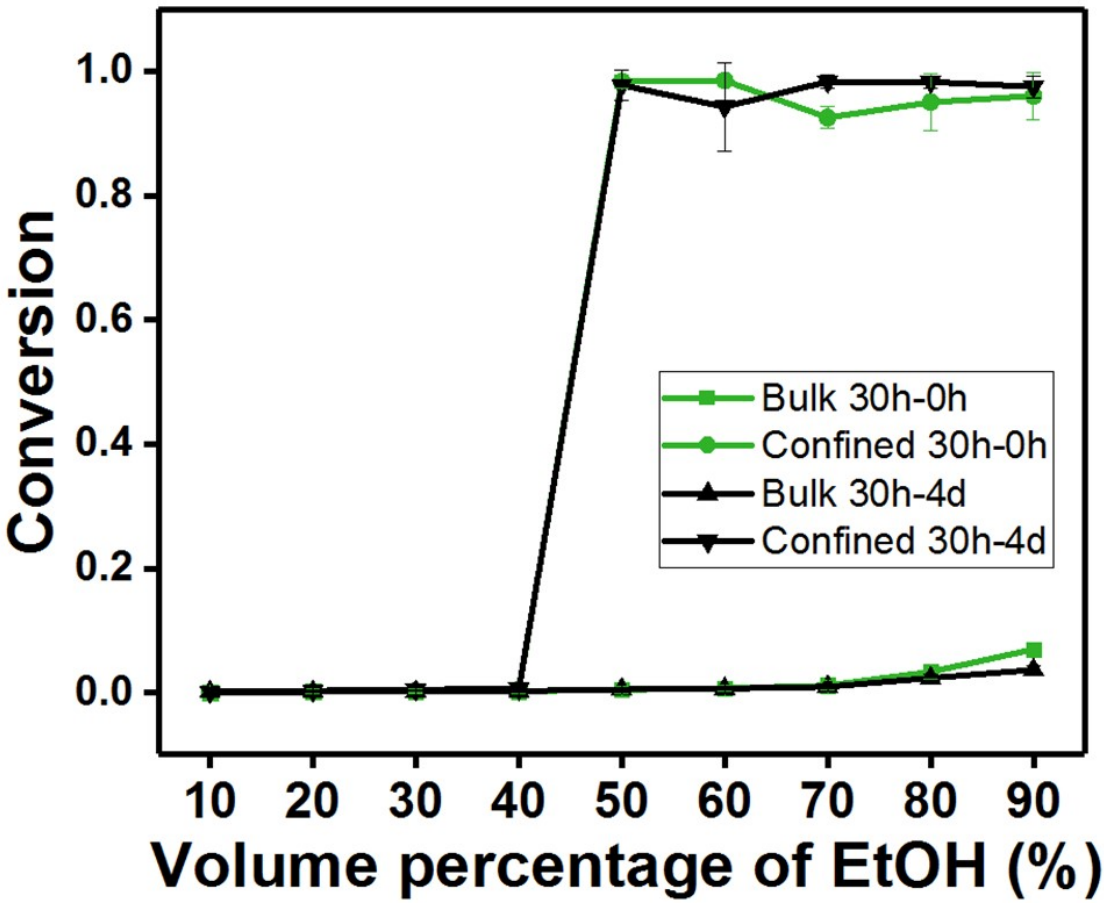

Fig. S10. **The bulk/confined catalytic performance measured in EtOH-DMF binary solvent with and without stabilization for 4 days.**

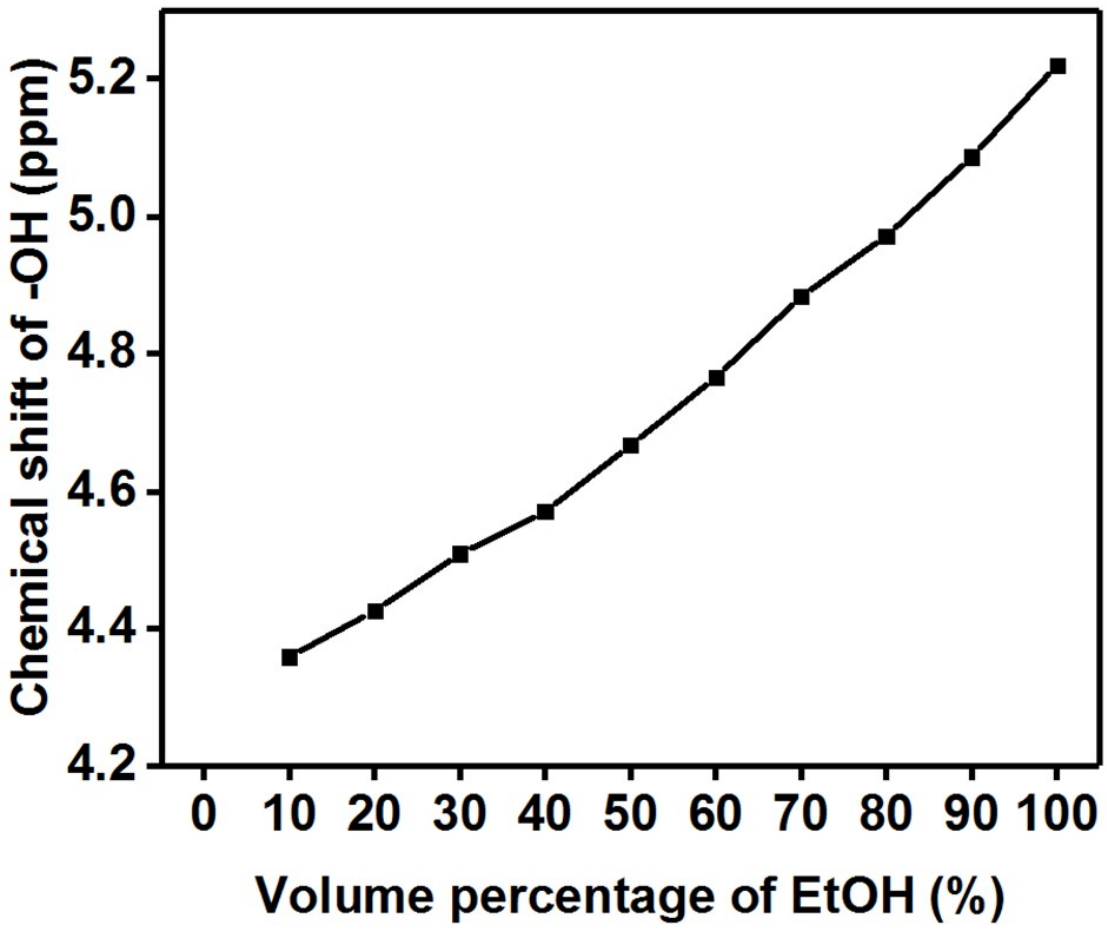

Fig. S11. Chemical shifts of the hydroxyl peaks of ethanol in EtOH-DMF binary solvent at 10% intervals.

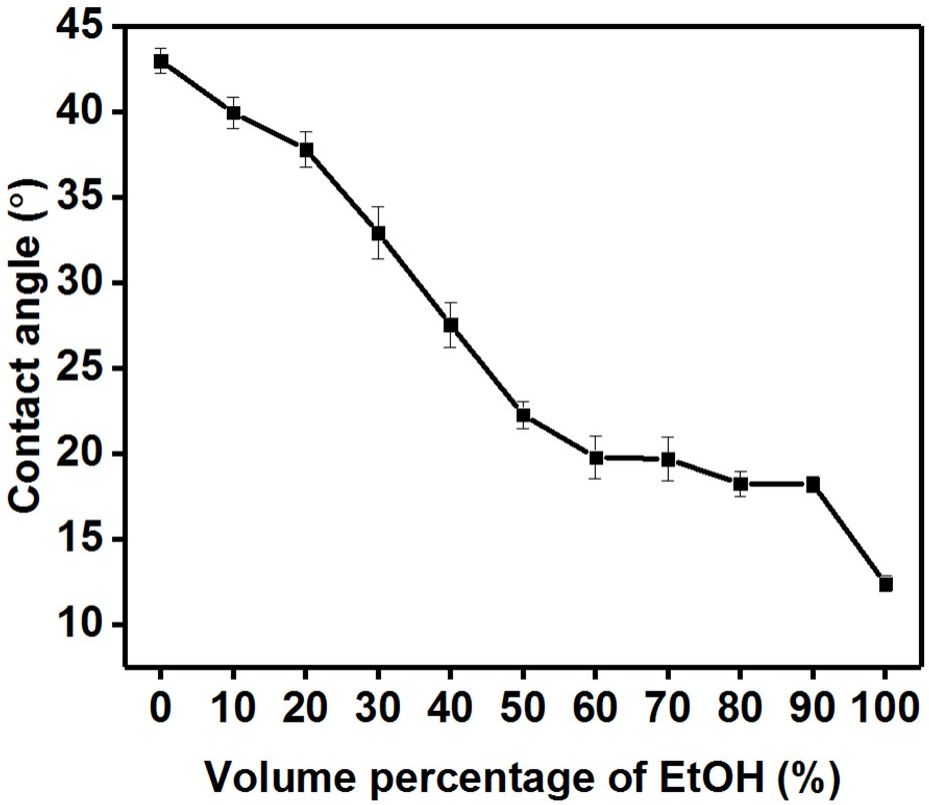

Fig. S12. CA of EtOH-DMF binary solvent at 10% intervals.

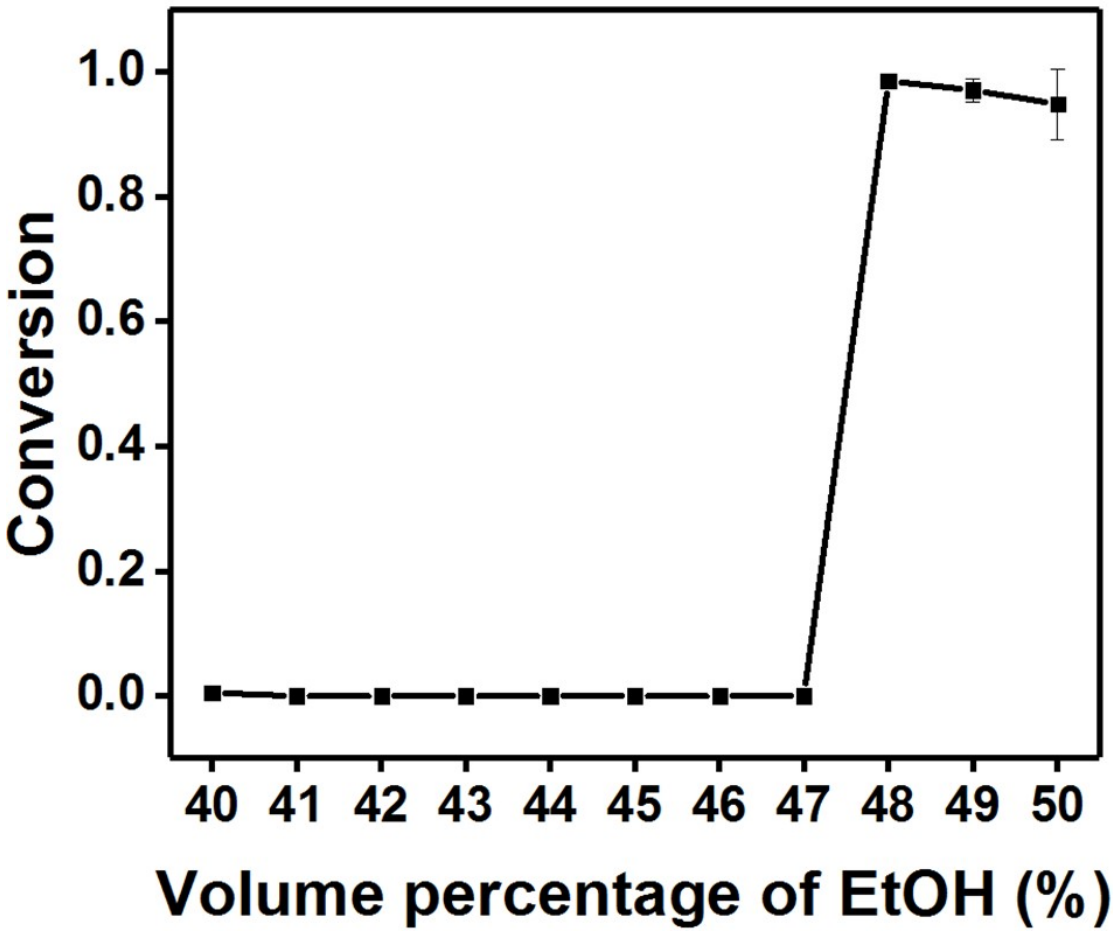

Fig. S13. Confined catalytic performance tested in EtOH-DMF binary solvent of ethanol content 40%-50% at 1% intervals.

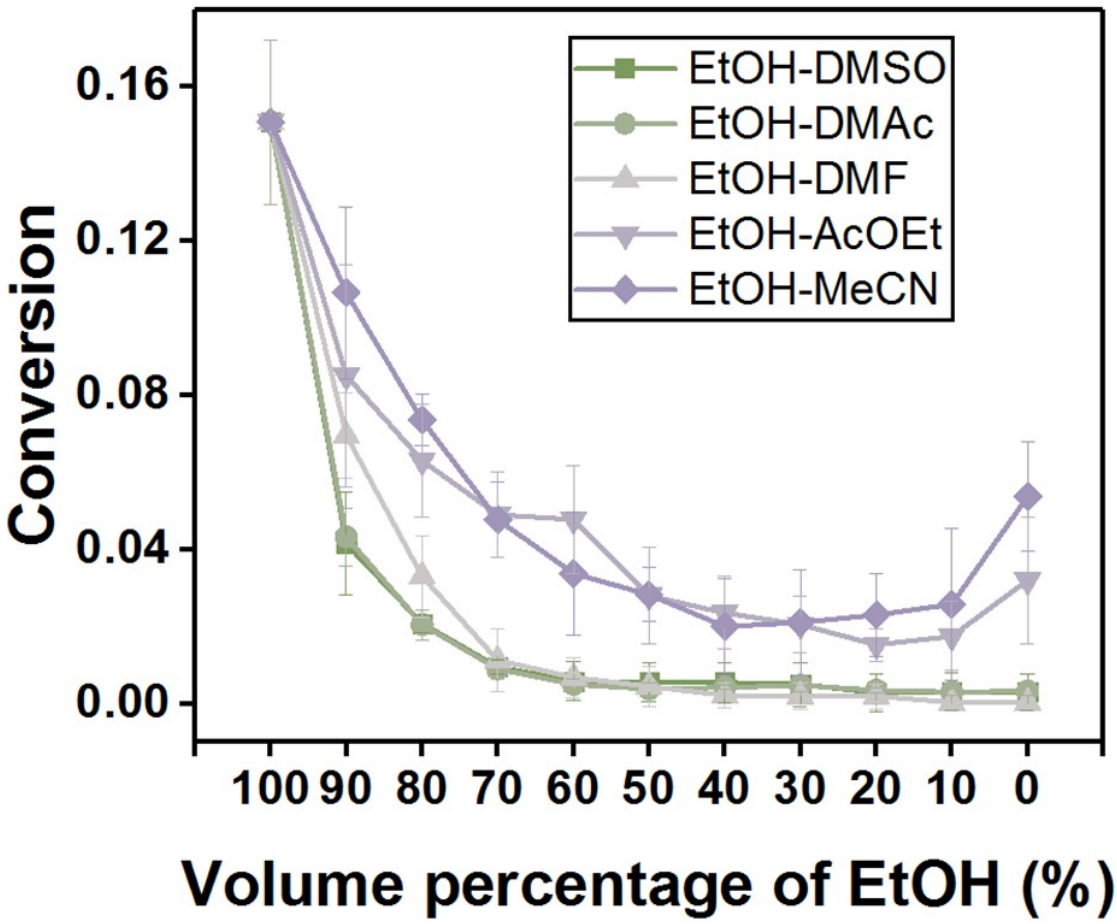

Fig. S14. **The trend of bulk reaction in five binary solvents as a function of the ethanol content.**

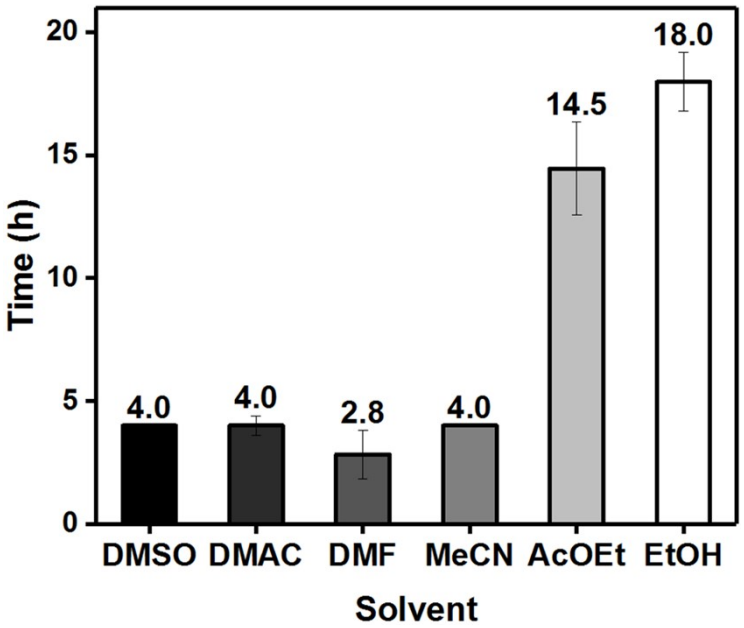

Fig. S15. **The time required for the 1 mL of reactant solution to fall completely into GOMR.**

The reactant solution was prepared with the six pure solvents, respectively

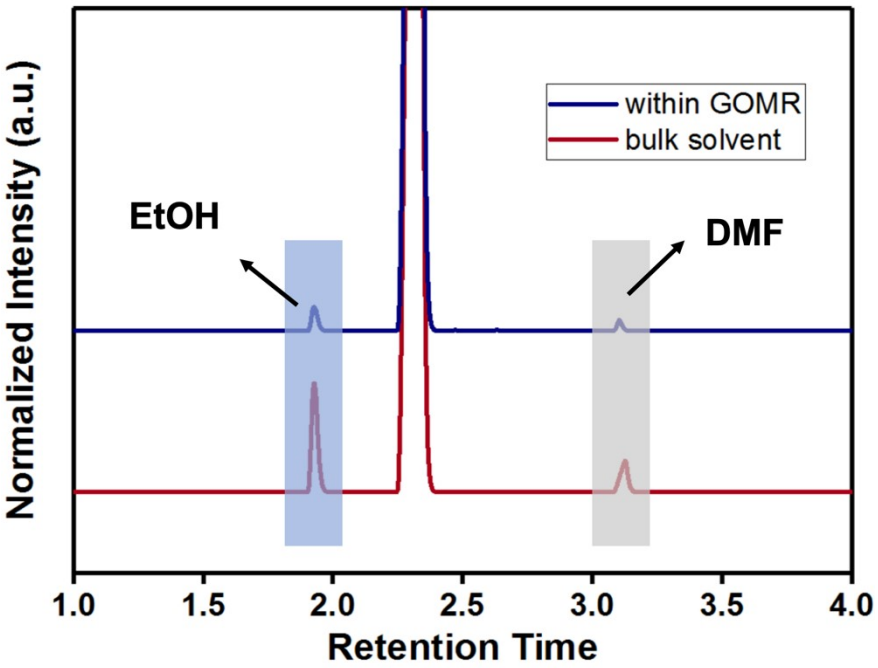

Fig. S16. **The composition difference test for binary solvent in bulk solvent or within the channel of GOMR.** EtOH-DMF (7:3) was taken as the representative example. 1 mL of EtOH-DMF (7:3) was added into GOMR and a negative pressure of 0.1 MPa was applied. After vacuum filtration at room temperature for 4 hours, the GOMR was carefully taken out and washed to eliminate any residual liquid on its surface. The obtained GOMR was then placed in 2 ml of ethyl acetate and subjected to ultrasonication for 1 minute to convert it back into GO powder. The mixture was vigorously shaken to ensure thorough dissolution of the solvents originally present within the channel of GOMR by the ethyl acetate. The resulting leachate was analyzed using gas chromatography, with a comparative analysis performed against the bulk solvent. For bulk solvent, the peak area ratio of ethanol to DMF was 3223507:1106489 (3.00:1). For GOMR leachate, this ratio was 666667:243741 (2.74:1). It was noted that the proportion of ethanol in GOMR leachate was slightly lower than that in bulk solvent. This discrepancy can be attributed to the much higher volatility of ethanol compared to DMF, coupled with the fact that liquid flow within the GOMR was driven by negative pressure. Near the outlet of channels of the GOMR, ethanol may begin to volatilize, leading to a slight reduction in its proportion in the leachate. We considered this deviation to be acceptable and therefore maintained that the liquid composition inside the GOMR channels was consistent with that of the bulk solution.

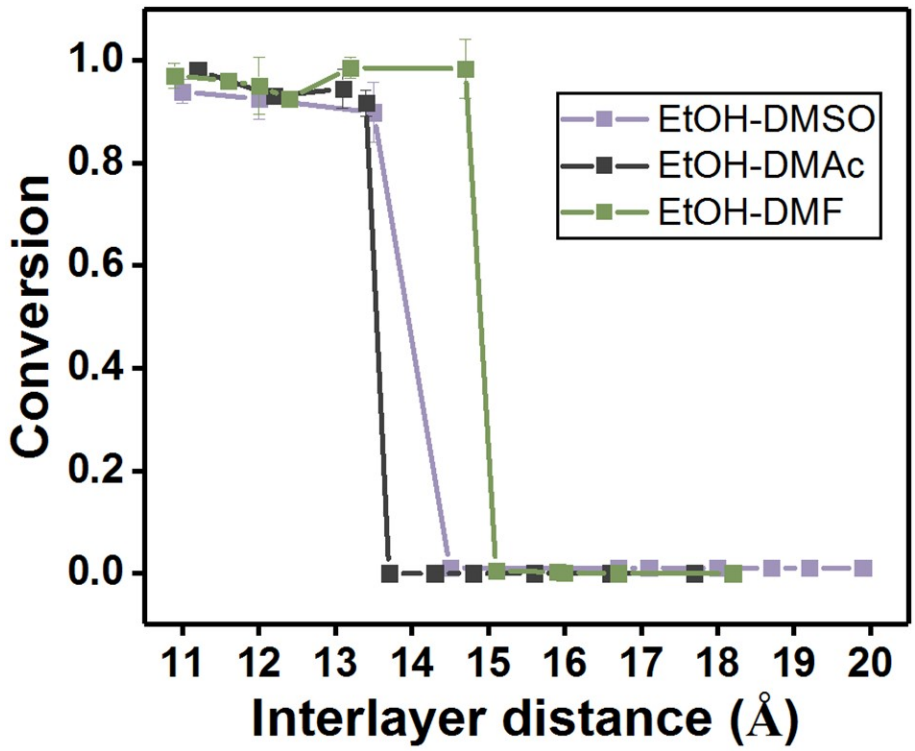

Fig. S17. The performance of confined catalysis in EtOH-DMF, EtOH-DMAC and EtOH-DMSO binary solvent as a function of the interlayer distance of GOMR.

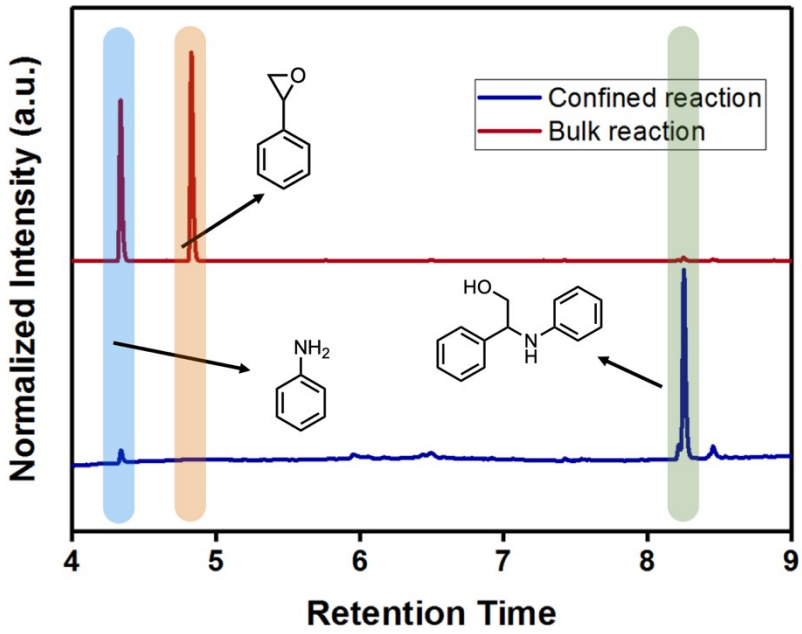

Fig. S18. Representative raw chromatograms of a case of confined reaction and bulk reaction. Using EtOH-DMF (8:2) as the solvent for both reactions.

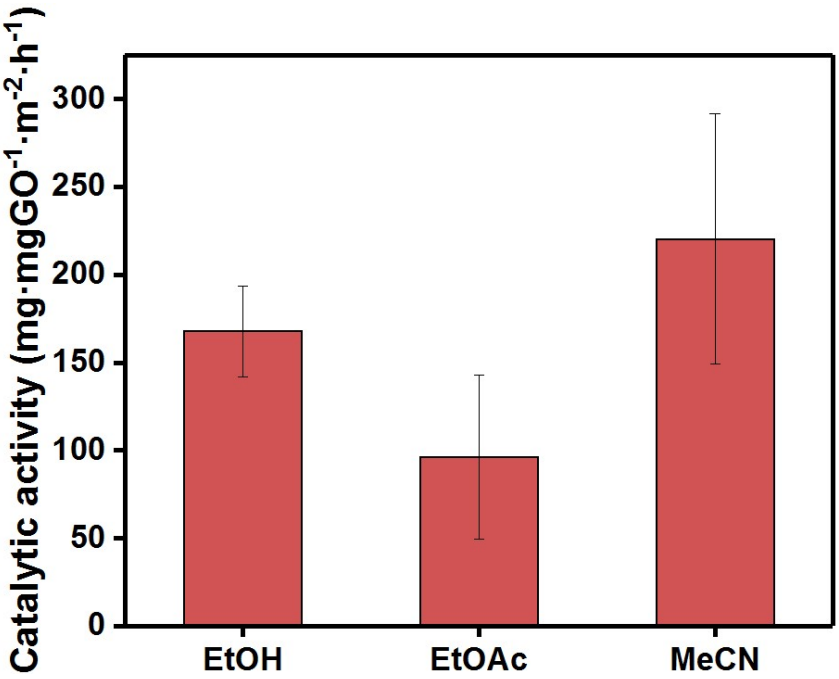

Fig. S19. Normalize catalytic activity by GO mass or surface area. The GO mass for each case to fabricate GOMR is 0.5mg. The diameter of the GOMR is 15mm, so the surface area is 177mm^2 (0.000177m^2). The time required for the 1 mL of reactant solution to fall completely into GOMR is shown in Fig.S15, and for EtOH, EtOAc and MeCN are 18.0h, 14.5h and 4.0h, respectively. Therefore, the normalized catalytic activity of GOMR in EtOH, EtOAc and MeCN are 167.83, 96.03 and 220.20 mg·mgGO^{-1}·m^{-2}·h^{-1}, respectively.

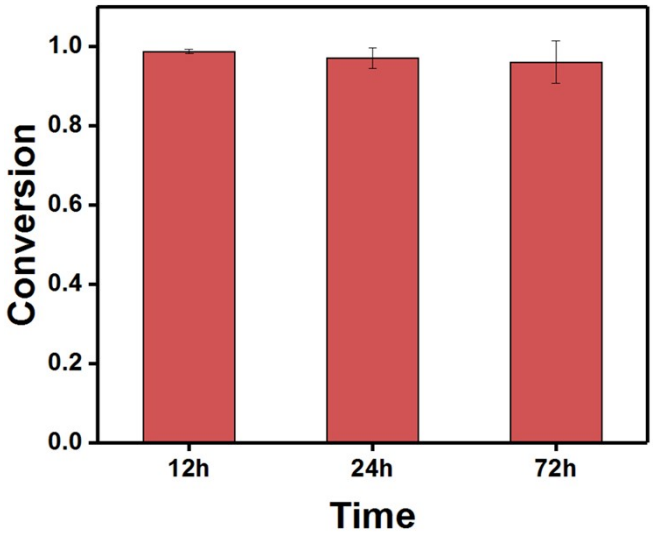

Fig. S20. The time-dependent catalytic performance of GOMR. The catalytic duration time of the GOMR was varied by adjusting the volume of the reactant solution. Catalytic performance of the GOMR was tested at 12h, 24h and 72h using ethanol as the solvent. The results showed no significant degradation, indicating that the catalytic activity of the GOMR could be remained over a period of 72 hours.

.

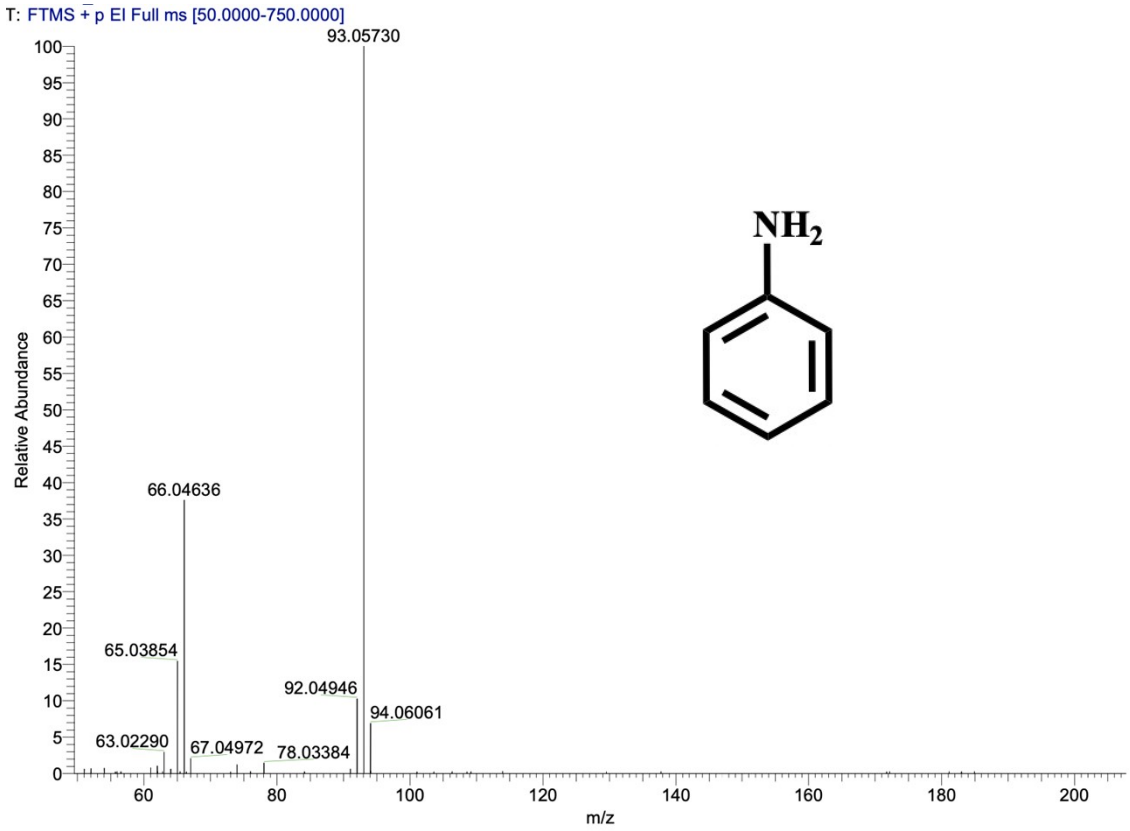

Fig. S21. Mass spectrum of aniline

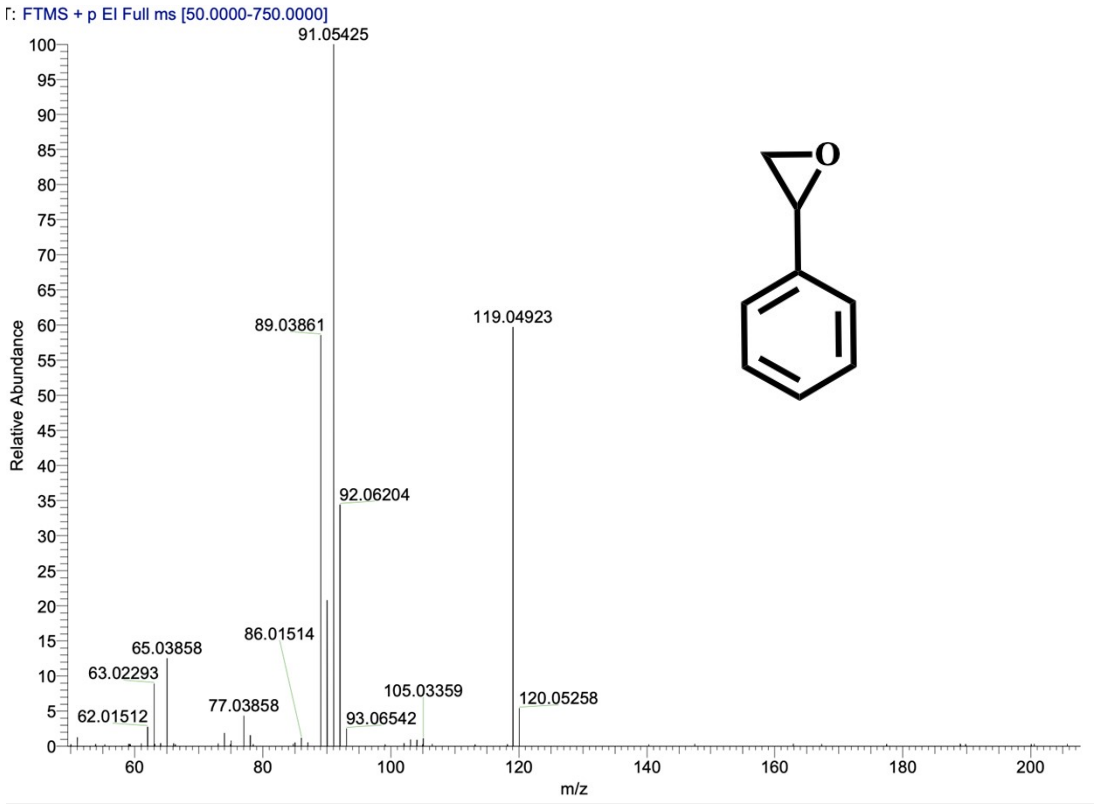

Fig. S22. Mass spectrum of styrene oxide.

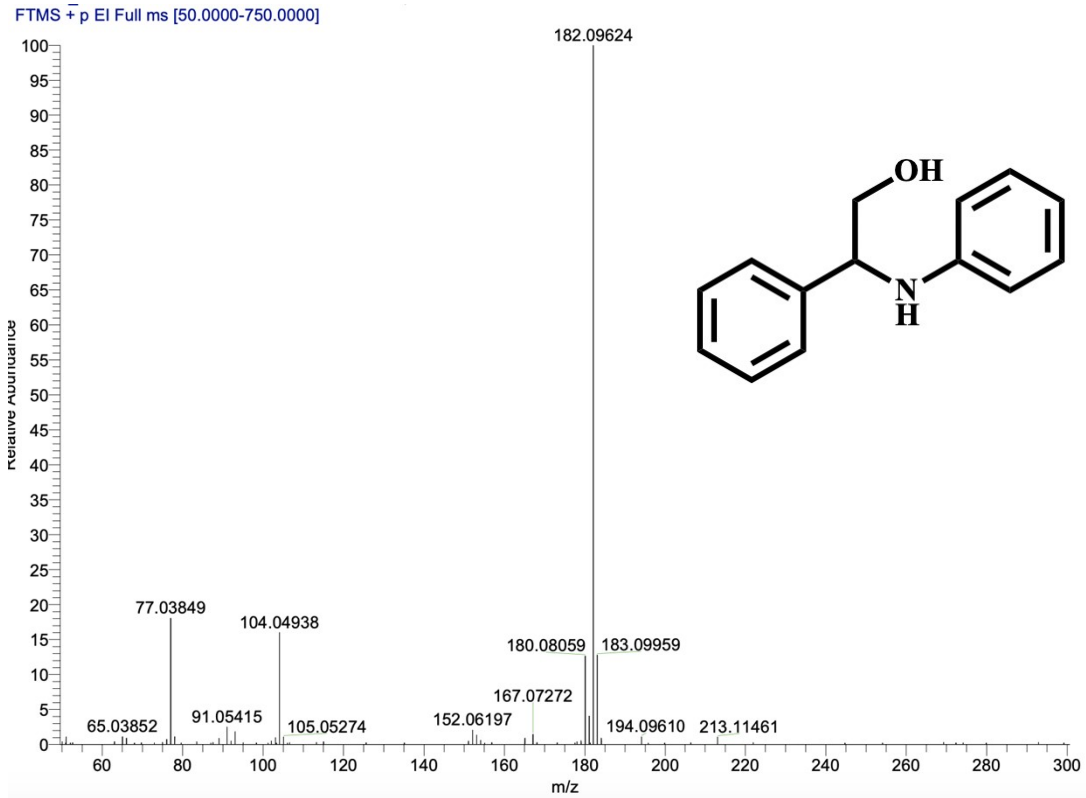

Fig. S23. **Mass spectrum of the product, 2-phenyl-2-(phenylamino) ethan-1-ol.**

REFRENCES:

1. https://jerkwin.github.io/gmxtools/model/graphene.html
2. L. Martínez, R. Andrade, E. G. Birgin and J. M. Martínez, *J. Comput. Chem.*, 2009, **30**, 2157-2164.
3. W. L. Jorgensen, D. S. Maxwell and J. Tirado-Rives, *J. Am. Chem. Soc.*, 1996, **118**, 11225-11236.
4. W. Xin, H. Xiao, X.-Y. Kong, J. Chen, L. Yang, B. Niu, Y. Qian, Y. Teng, L. Jiang and L. Wen, *ACS Nano*, 2020, **14**, 9701-9710.
5. Y. Hu, H. Xiao, L. Fu, P. Liu, Y. Wu, W. Chen, Y. Qian, S. Zhou, X.-y. Kong, Z. Zhang, L. Jiang and L. Wen, *Adv. Mater.*, 2023, **35**, 2301285.
6. M. J. Abraham, T. Murtola, R. Schulz, S. Páll, J. C. Smith, B. Hess and E. Lindahl, *SoftwareX*, 2015, **1-2**, 19-25.
7. S. Páll, M. J. Abraham, C. Kutzner, B. Hess and E. Lindahl, *Lect. Notes Comput. Sci*, 2015, **8759**, 3-27.
8. S. Pronk, S. Páll, R. Schulz, P. Larsson, P. Bjelkmar, R. Apostolov, M. R. Shirts, J. C. Smith, P. M. Kasson, D. van der Spoel, B. Hess and E. Lindahl, *Bioinformatics*, 2013, **29**, 845-854.
9. B. Hess, C. Kutzner, D. van der Spoel and E. Lindahl, *J. Chem. Theory Comput.*, 2008, **4**, 435-447.
10. D. Van Der Spoel, E. Lindahl, B. Hess, G. Groenhof, A. E. Mark and H. J. C. Berendsen, *J. Comput. Chem.*, 2005, **26**, 1701-1718.
11. E. Lindahl, B. Hess and D. van der Spoel, *Molecular modeling annual*, 2001, **7**, 306-317.
12. H. J. C. Berendsen, D. van der Spoel and R. van Drunen, *Comput. Phys. Commun.*, 1995, **91**, 43-56.